Chaining dynamics of a pair of ellipsoidal micro-particles under a uniform magnetic field

Jie Zhang[1], Cheng Wang[1]
1. Department of Mechanical and Aerospace Engineering, Missouri University of Science and Technology, Rolla, MO, USA

Abstract: In this work, we numerically investigate particle-particle interactions and relative motions of a pair of paramagnetic elliptical particles by using the direct numerical simulations that resolve the magnetic and flow fields around the finite sized particles. The modeling is based on the finite element method and arbitrary Lagrangian-Eulerian approach with full consideration of particle-fluid-magnetic field interaction. The effects of initial position and aspect ratio of the particles are investigated. The results show that larger initial relative angles and distances, and larger aspect ratios tend to require more time to form a stable chain.

Keywords: Microfludics, CFD, FSI, magnetic field

1. Introduction

Due to particle interactions, magnetic particles suspended in non-magnetic field tend to form chains, clusters or columns under magnetic fields. The non-spherical magnetic particles in the suspension show different rheological properties compared to spherical particles. A pair of magnetic particles suspended in a quiescent fluid is a basic model to investigate the particle-particle interactions in particle suspensions. There are some numerical investigations on the motion of magnetic spherical particles under the magnetic field. The particle-based numerical method are the most popular one, which is based on point-dipole approximation and stokes drag law [1-3]. The particle is modeled as a dipole point and the dipole-dipole model is applied to study the particle-particle interactions between the particles. However, particle-particle interactions due to the hydrodynamic and magnetic effects are neglected in this method, which may result in the quantitatively inaccurate or even erroneous results. More precise models are introduced to investigate the field-induced coupling and hydrodynamic interactions between the particles. Keaveny and Maxey [4] reported a dipole model including the locally higher-order multipoles to resolve the near-field magnetic interactions between two paramagnetic particles. To consider both hydrodynamic and magnetic interactions between the particles, Gao et al. [5] reported a particle-based numerical scheme by using magnetic dipole moments and extended forms of the Oseen-Burgers tensor to study the dynamics of magnetic particle chains in a viscous fluid under the rotating magnetic field. Their numerical results are qualitatively and quantitatively in agreement with the results obtained from video-microscopy experiments. Kang et al. [6, 7] presented a direct numerical simulation model based on finite element method (FEM) and fictitious domain method to solve both two-and three-dimensional flow problems with paramagnetic particles in a non-magnetic fluid under both uniform and rotating magnetic field. The magnetic force acting on the particles are computed through the divergence of Maxwell stress tensor, and works as a body force applied to the momentum equation. Suh and Kang [8, 9] introduced a direct numerical simulation model based on immersed-boundary finite volume method to solve two-dimensional motion of paramagnetic particles in a viscous fluid under the uniform magnetic field. They have the similar particle trajectories of two magnetic particles under the uniform magnetic field as two-dimensional simulations in Kang's paper [6].

In this study, we developed a transient multi-physics numerical model to investigate the particle-particle interactions and relative motions of a pair of paramagnetic elliptical particles under a uniform magnetic field. Numerical simulations will be performed by direct numerical simulation (DNS) based on finite element method and arbitrary Lagrangian-Eulerian (ALE) approach. The fluid field, magnetic field and particle motion are coupled and solved by using moving mesh based on ALE approach. The effect of some important factors such as particle initial position and aspect ratio on particle-particle interactions and relative motions will be investigated.

2. Simulation method

2.1 Mathematical model

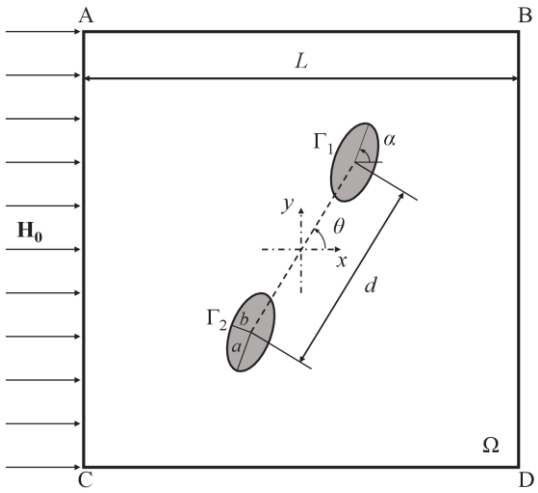

Figure 1. Schematic of numerical model of a pair of elliptical particles suspended in a quiescent flow under a uniform magnetic field $\mathbf{H_0}$.

We consider a pair of identical rigid prolate elliptical particles immersed in a quiescent Newtonian fluid in a square domain with density ρ_f and dynamic viscosity η_f as shown in Figure 2. Ω represents the entire computational domain, which includes fluid and two particle domains. Γ_1 and Γ_2 are the particle surfaces of those two particles. The center of the square is set as the origin of the Cartesian coordinate system. Two particles are set as axis-symmetric to the center of the square with the center-to-center distance of d and the relative angle of θ with respect to the positive x-axis. The particle aspect ratio is $r_p = a/b$, where a and b are the major and minor semi-axis lengths of particles, respectively. The length of the computational domain is L. The orientation angle of the particle, α, is defined as the angle between the major axis of the particle and the positive x-axis. A uniform magnetic field, $\mathbf{H_0}$, is applied at the positive x direction.

The fluid is considered as an incompressible, Newtonian, and non-magnetic with magnetic susceptibility of χ_f. The particles are paramagnetic with magnetic susceptibility of χ_p. The flow field, $\mathbf{u}$, is governed by the continuity equation and Navier-Stokes equation:

$$\nabla \cdot \mathbf{u} = 0,$$
$$\rho_f \left[\frac{\partial \boldsymbol{u}}{\partial t} + (\mathbf{u}\cdot\nabla)\mathbf{u}\right] = \nabla \cdot [-p\boldsymbol{I} + \eta_f(\nabla\mathbf{u} + (\nabla\mathbf{u})^T)], \quad (1)$$

where p and t are the pressure and the time, respectively.

No-slip condition is set on the particle surface, so the fluid velocities on the particle surface Γ_1 and Γ_2 are given as:

$$\mathbf{u_i} = \mathbf{U}_{pi} + \boldsymbol{\omega}_{pi} \times (\mathbf{x}_{si} - \mathbf{x}_{pi}), \quad (5)$$

where i = 1 and 2 representing the first and second particle. $\mathbf{U}_{pi}$ and $\boldsymbol{\omega}_{pi}$ are the translational and rotational velocities of the ith particle, respectively. $\mathbf{x}_{si}$ and $\mathbf{x}_{pi}$ are the position vectors of the surface and the center of the ith particle. The hydrodynamic force and torque acting on the particle are expressed as:

$$\mathbf{F}_{\mathrm{Hi}} = \int (\boldsymbol{\tau}_{\mathrm{Hi}} \cdot \mathbf{n}) dS, \quad (6)$$
$$\mathbf{T}_{\mathrm{Hi}} = \int [\boldsymbol{\tau}_{Hi} \times (\mathbf{x}_{si} - \mathbf{x}_{pi}) \cdot \mathbf{n}] dS, \quad (7)$$

where $\boldsymbol{\tau}_{Hi} = -p\boldsymbol{I} + \eta_f(\nabla\boldsymbol{u_i} + (\nabla\boldsymbol{u_i})^T)$ is the hydrodynamic stress tensor on the surface of the ith particle.

The governing equations of the uniform magnetic field are given as:

$$\mathbf{H} = -\nabla V_m,$$
$$\nabla \cdot \mathbf{H} = 0, \quad (8)$$

where V_m is the magnetic potential. The magnetic potential difference to generate the magnetic field is set on the top and bottom wall (AB and CD). Magnetic insulation boundary condition is applied on the left and the right boundaries (AC and BD) of the computational domain.

The magnetic force and torque acting on the particles are expressed as [10]:

$$\mathbf{F}_{\mathrm{mi}} = \int (\boldsymbol{\tau}_{mi} \cdot \mathbf{n}) d\Gamma_i, \quad (9)$$
$$\mathbf{T}_{\mathrm{mi}} = \int [\boldsymbol{\tau}_{mi} \times (\mathbf{x}_{si} - \mathbf{x}_{pi}) \cdot \mathbf{n}] dS$$

where $\boldsymbol{\tau}_{mi} = \mu(\mathbf{HH} - \frac{1}{2}H^2\mathbf{I})$ is Maxwell stress tensor on the ith particle surface Γ_i, $\mathrm{H}^2 = \mathbf{H}\cdot\mathbf{H}$, $\mathbf{I}$ is the identity tensor.

The translation and rotation of the particles are governed by Newton's second law and Euler's equation:

$$m_{pi}\frac{d\boldsymbol{U}_{pi}}{dt} = \boldsymbol{F}_{Hi} + \boldsymbol{F}_{mi}, \quad (10)$$
$$I_{pi}\frac{d\boldsymbol{\omega}_{pi}}{dt} = \boldsymbol{T}_{Hi} + \boldsymbol{T}_{mi}, \quad (11)$$

where m_{pi} and I_{pi} are the mass and the moment of inertia of the ith particle. At each time step, the position of center $\mathbf{C_{pi}}(t) = (x_{\mathrm{pi}}, y_{\mathrm{pi}})$ and orientation $\alpha_{\mathrm{pi}}(t) = \alpha(t)$ of the ith particle are expressed as:

$$\boldsymbol{C_{pi}}(t) = \boldsymbol{C_{pi}}(0) + \int_0^t \boldsymbol{U}_{pi}(s)ds, \quad (12)$$
$$\alpha_{pi}(t) = \alpha_{pi}(0) + \int_0^t \omega_{pi}(s)ds, \quad (13)$$

where $\boldsymbol{C_{pi}}(0)$ and $\alpha_{pi}(0)$ are the initial position and orientation of the ith particle.

Here, particle position (x, y) and center-to-center distance d is dimensionless by the particle equivalent radius, R_0, i.e. $x^* = x/R_0$, $y^* = y/R_0$ and $d^* = d/R_0$. The dimensionless time is defined as $t^* = t/\tau_m$. For a linear magnetization of the particle we considered in this work, $\tau_m = \eta_f/(\mu_0\chi_f^2 H_0^2)$ is referred to as the magnetoviscous time constant[11], which represents a characteristic time to measure the relative effect between viscous and magnetic stresses.

2.2. COMOL settings

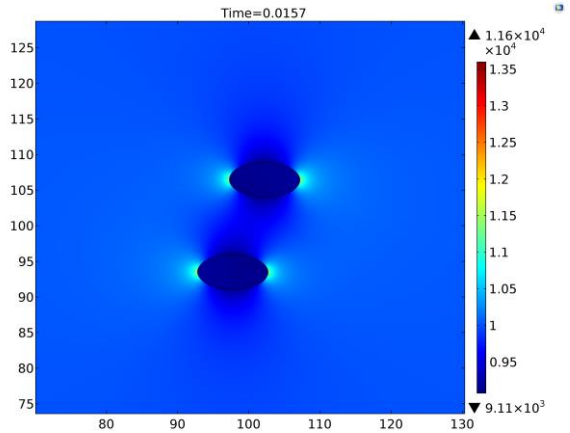

Figure 2. Magnetic field around a pair of elliptical particles with r_p=2 under uniform magnetic field of H_0=10000A/m.

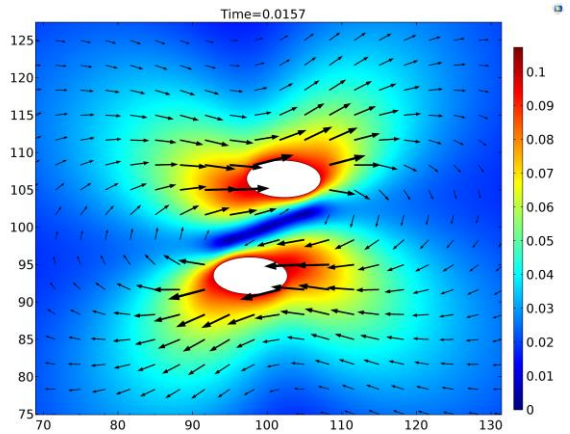

Figure 3. Induced velocity around a pair of elliptical particles with r_p=2 under uniform magnetic field of H_0=10000A/m.

To fully couple flow field, magnetic field and particle motion, Fluid-structure Interaction (FSI) and Magnetic Field, No Currents (mfnc) modules are coupled in COMSOL Multiphysics® software. The direct numerical simulation (DNS) based on finite element method (FEM) and arbitrary Lagrangian-Eulerian (ALE) approach is used to calculate the magnetic field, flow field and particle motions at the same time. The two-way coupling of particle-fluid-magnetic interaction model is solved by using a time-dependent solver through the ALE method, which solves the magnetic field in the entire domain, the fluid field in an Eulerian (deformed) frame, and tracks the particle motion in a Lagrangian (undeformed) frame at the same time. Figure 2 shows the magnetic field around two elliptical particles with r_p = 2 in the computational domain under the magnetic field of H_0 = 10000A/m.

Modelling of FSI is realized by combining Laminar Flow component in Fluid Flow module, Solid Mechanics component in Structural Mechanics module and Moving Mesh component in Mathematics module. Figure 4 shows the induced velocity around a pair of elliptical particles with r_p = 2 under uniform magnetic field of H_0=10000A/m.

The moving meshing interface is used to track the deformation of the fluid domain where the meshes are free to deform. The meshes of particle domain are fixed which is determined by their trajectories and orientations. As the mesh deforms, the mesh distortion is increased. When the distortion value is increased to 0.3, the re-meshing process initiates.

In this simulation, we used quadratic triangular elements in the entire domain. To accurately calculate the hydrodynamic force and torque, as well as magnetic force and torque acting on the particle, fine meshes are applied around the particle surfaces and finer meshes are applied around the tips of the particles. The total number of elements was about 16,000 in the entire domain and about 120 elements on each particle surface to obtain stable and mesh-independent results.

2.3 Material properties

In this study, the fluid and particles in the simulations are water and polystyrene particles respectively. The density and dynamic viscosity of water are 1000 kg/m^3 and 1.002 × 10^{-3} Pa·s respectively. The magnetic susceptibilities of fluid and particle are 0 and 0.26 respectively. The density of particle is 1100 kg/m^3. The particles used in the simulation have varying aspect ratios, but have the same volume, which is equivalent to a 3.5 μm-radius (R_0) sphere, and the side length of the square domain is 50R_0, which is large enough for this work. The magnetic field strength is H_0 = 10,000 A/m.

3. Results and Discussion

3.1. Orientation of a single prolate elliptical particle

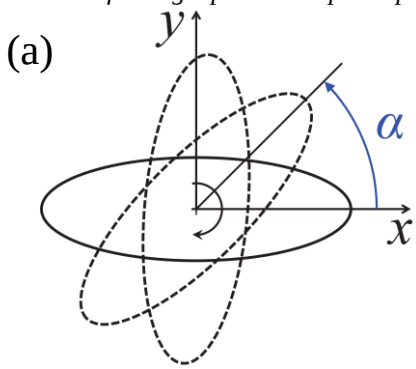

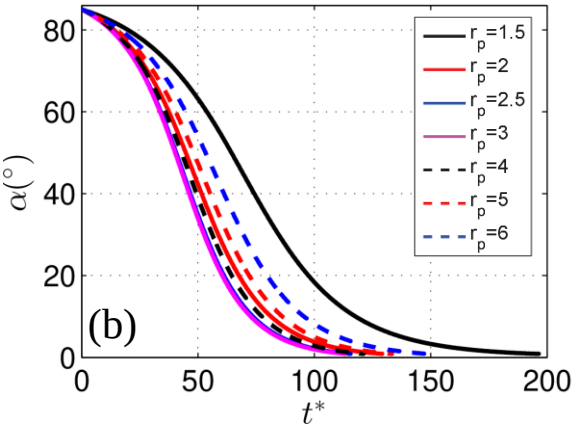

Figure 4. (a) A diagram of the magneto-orientation process for r_p = 3 when the magnetic field is directed left to right; (b) the self-orientation angle of a single prolate elliptical particle, α, as a function of dimensionless time, t^*, for different aspect ratios.

In this section, we investigate the magneto-orientation of a single prolate elliptical paramagnetic particle under a uniform magnetic field. Figure 4b shows the simulation result of the orientation angle of the particle, α, of a single elliptical particle varying with the dimensionless time, t^* for different aspect ratio, where the initial angle between the major axis of the particle and the magnetic field α_0 = 85˚. To compare the effect of aspect ratio on the particle rotation, the relaxation time is defined as the time required for the particle rotating from initial angle to the orientation angle α falling below 1% of its initial angle. From the figure 4b, we can see the effect of aspect ratio, r_p, on the dimensionless relaxation time, t^*. For a circular particle, there is no net magnetic torque acting on the particle under a uniform magnetic field, so the relaxation time is considered as infinite. For a nearly circular particle, we can except it has a larger relaxation time due to a smaller torque acting on the particle. From the figure 4b, we can see that the relaxation time of the particle with aspect ratio r_p = 1.5 is the longest among these seven cases. The relaxation time is reduced when r_p increases from 1.5 to 3 as shown in the solid line in Figure 4b. We also can see that the minimum relaxation time is achieved when r_p = 3 among those seven cases. As aspect ratio continues to increase, the relaxation time is increased as shown in the dash line in Figure 4b. Those results have quantitative agreement with the theory from Ref. [11], where the relaxation time is first decreased and then increased as the aspect ratio is increased.

3.2. Orientation of a pair of elliptical particles

To systematically investigate the global reorientation of two particles, the effect of some important factors on the particle-particle interaction will be studied in the following subsections.

3.2.1 The effect of initial relative angle

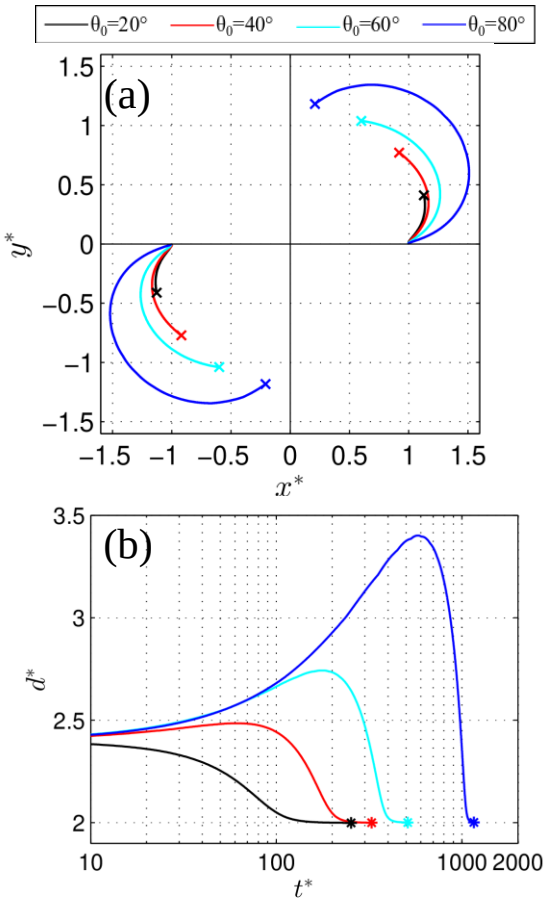

Figure 5. The effect of initial relative orientation angle between the particles on the particle-particle interaction. (a) Trajectories of particle centers, (b) center-to-center distance varying with dimensionless time when r_p = 2 and d_0^* = 2.4 for initial relative angle θ_0 = 20˚, 40˚, 60˚ and 80˚.

First, we investigate the effect of initial relative angle between two particles, θ_0, on the particle-particle interaction. Initially, the particles with aspect ratio r_p = 2 are placed at (x^*, y^*) = [±2.4cos(θ_0); ±2.4sin(θ_0)] for different initial center-to-center distance, θ_0, as shown as cross dots in Figure 7(a). As can be seen in Figure 5(a) and (b), the particles spend more time for the whole process, and particle trajectory becomes longer as θ_0 increases from 20˚ to 80˚. We can see from Figure 5(b) that, when the initial orientation angle θ_0 = 80˚ and 60˚, the dimensionless center-to-center distance, d^*, first increases and then decreases with dimensionless time, t^*; when θ_0 = 20˚, d^* decreases with t^*. However, when θ_0 = 40˚, the dimensionless distance varying with dimensionless

time has the similar result as θ_0 = 80° and 60°: d^* first increases and then decreases with t^*. It means that the critical angle, θ_c, of the elliptical particles with r_p = 2 is smaller than 40°, which is different from the critical angle of circular particles[9]. In addition, as θ_0 increases, the increasing and decreasing rates become steeper and the maximum of d^* become larger.

3.2.2. The effect of initial center-to-center distance

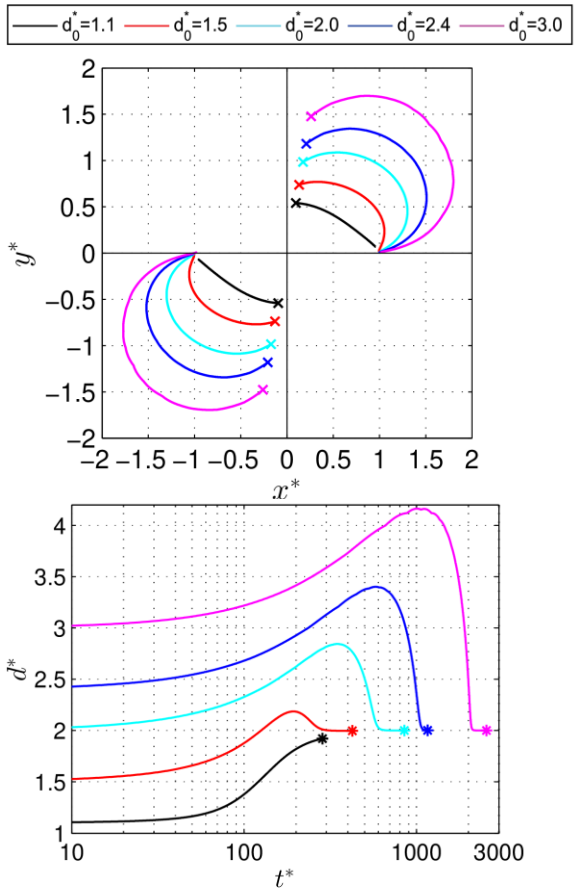

Figure 6. The effect of initial center-to-center distance on the particle-particle interaction. (a) Trajectories of particle centers, (b) center-to-center distance varying with dimensionless time when r_p = 2 and θ_0 = 80° for initial relative distance d_0^* = 1.1, 1.5, 2.0, 2.5 and 3.0.

Then, we investigate the effect of initial center-to-center distance between two particles, d_0^*, on the particle-particle interaction. Initially, the particles with aspect ratio r_p = 2 are placed at (x^*, y^*) = [$\pm d_0^*\cos(80°)$, $\pm d_0^*\sin(80°)$] when initial center-to-center distance, d_0^*, varies from 1.1 to 3.0 as shown as cross dots in Figure 6(a). As can be seen from Figure 6(a) and (b), the particles spend more time for the whole process and particle trajectory becomes longer when d_0^* increases from 1.1 to 3.0. There is a similar result for d_0^* as we discussed in Section 3.2.1: it first increases and then decreases with t^* when d_0^* = 1.5, 2.0, 2.4 or 3.0. The result is different for d_0^* = 1.1: it increases monotonously with t^*. Figure 6(b) demonstrates that the magnetic torque has much more influence on the particle-particle interaction when the two particles are too close. In addition, the change rule for d_0^* = 1.1 is also different: it has just one increasing-and-decreasing circle, while other relative distances have the similar results as in Section 3.2.1: two increasing-and-decreasing circles happens.

3.2.3. The effect of particle aspect ratio

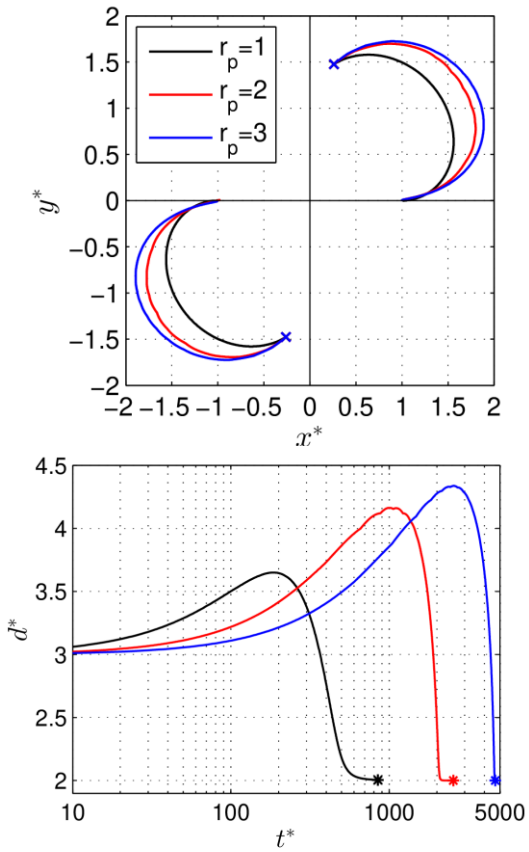

Figure 7. The effect of particle aspect ratio on the particle-particle interaction. (a) Trajectories of particle centers, (b) center-to-center distance varying with dimensionless time when d_0^* = 3.0 and θ_0 = 80°.

Here, we investigate the effect of particle aspect ratio, r_p, on the particle-particle interaction. Initially, the particles are placed at (x^*, y^*) = [$\pm 2.4\cos(80°)$, $\pm 2.4\sin(80°)$] when particle aspect ratio, r_p, varies from 1 to 3 as shown as cross dots in Figure 7. To compare the effect of r_p on the particle-particle interaction, the particle trajectories and the center-to-center distance are dimensionless by its major semi-axis length a. Figure 7(a) and (b) show the particle trajectories and particle center-to-center distance for

r_p = 1, 2 and 3. We can see that, as r_p becomes larger, the particle trajectory becomes longer and the particles spend more time for the whole process. What's more, the maximum of d^* becomes larger and the overall increasing rate from beginning to the maximum becomes smaller as r_p becomes larger.

4. Conclusions

The particle-particle interactions and relative motions of a pair of paramagnetic particles of elliptical shapes are numerically investigated using direct numerical simulations based on the finite element method and arbitrary Lagrangian-Eulerian approach. The numerical modeling considers the particle-fluid-magnetic field interaction. The rotational dynamics of a single elliptical paramagnetic particle is first investigated. The simulation results are in quantitative agreement with the theory in Shine and Armstrong's paper [11]. We focused our simulations on the relative motion of a pair of particles when initial orientation angle is parallel to the direction of magnetic field. Based on this model, we investigated the influence of the initial relative angle and distance of the particles, aspect ratio on the particle-particle interactions and relative motions of two particles. The results show that the particles of larger initial relative angles and distances need more time to form a stable chain and smaller final particle and relative orientation angles. For a larger particle aspect ratio, more time is required to form a chain, and the final particle and the relative orientation angles are larger. Therefore, this work provides useful information for the fundamental particle-particle interactions mechanism in the magnetic particle suspensions under a uniform magnetic field.

References

[1] S. Melle and J. E. Martin. Chain model of a magnetorheological suspension in a rotating field. The Journal of chemical physics, 118(21):9875-9881, 2003.

[2] I. Petousis, E. Homburg, R. Derks, and A. Dietzel. Transient behaviour of magnetic micro-bead chains rotating in a fluid by external fields. Lab on a Chip, 7(12):1746-1751, 2007.

[3] D. C. Stuart, C. Kleijn, and S. Kenjereˇs. An efficient and robust method for lagrangian magnetic particle tracking in fluid flow simulations on unstructured grids. Computers & Fluids, 40(1):188-194, 2011.

[4] E. E. Keaveny and M. R. Maxey. Modeling the magnetic interactions between paramagnetic beads in magnetorheological fluids. Journal of Computational Physics, 227(22):9554-9571, 2008.

[5] Y. Gao, M. Hulsen, T. Kang, and J. Den Toonder. Numerical and experimental study of a rotating magnetic particle chain in a viscous fluid. Physical Review E, 86(4):041503, 2012.

[6] T. G. Kang, M. A. Hulsen, J. M. den Toonder, P. D. Anderson, and H. E. Meijer. A direct simulation method for flows with suspended paramagnetic particles. Journal of Computational Physics, 227(9):4441-4458, 2008.

[7] T. G. Kang, Y. Gao, M. A. Hulsen, J. M. den Toonder, and P. D. Anderson. Direct simulation of the dynamics of two spherical particles actuated magnetically in a viscous fluid. Computers & Fluids, 86:569-581, 2013.

[8] S. Kang and Y. Suh. Direct simulation of flows with suspended paramagnetic particles using one-stage smoothed profile method. Journal of Fluids and Structures, 27(2):266-282, 2011.

[9] Y. K. Suh and S. Kang. Motion of paramagnetic particles in a viscous fluid under a uniform magnetic field: benchmark solutions. Journal of Engineering Mathematics, 69(1):25-58, 2011.

[10] J. A. Stratton. Electromagnetic theory. John Wiley & Sons, 2007.

[11] A. Shine and R. Armstrong. The rotation of a suspended axisymmetric ellipsoid in a magnetic field. Rheologica Acta, 26(2):152-161, 1987.

Acknowledgements

The authors gratefully acknowledge the financial support from the Department of Mechanical and Aerospace Engineering at Missouri University of Science and Technology.